ACS APPLIED MATERIALS & INTERFACES

Research Article

www.acsami.org

Substrate-Induced Phase of a [1]Benzothieno[3,2-*b*]benzothiophene Derivative and Phase Evolution by Aging and Solvent Vapor Annealing

Andrew O. F. Jones,*[,†] Yves H. Geerts,[‡] Jolanta Karpinska,[‡] Alan R. Kennedy,[∥] Roland Resel,[§] Christian Röthel,[§] Christian Ruzié,[‡] Oliver Werzer,[¶] and Michele Sferrazza[†]

[†]Département de Physique, Faculté des Sciences, Université Libre de Bruxelles CP223, Campus de la Plaine, 1050 Brussels, Belgium

[‡]Laboratoire de Chimie des Polymères, Faculté des Sciences, Université Libre de Bruxelles CP206/01, Campus de la Plaine, 1050 Brussels, Belgium

[∥]Department of Pure and Applied Chemistry, University of Strathclyde, 295 Cathedral Street, Glasgow G1 1XL, Scotland

[§]Institute of Solid State Physics, Graz University of Technology, Petersgasse 16, 8010 Graz, Austria

[¶]Institute of Pharmaceutical Sciences, Department of Pharmaceutical Technology, Karl-Franzens Universität Graz, Universitätsplatz 1, 8010 Graz, Austria

Supporting Information

ABSTRACT: Substrate-induced phases (SIPs) are polymorphic phases that are found in thin films of a material and are different from the single crystal or "bulk" structure of a material. In this work, we investigate the presence of a SIP in the family of [1]benzothieno[3,2-*b*]benzothiophene (BTBT) organic semiconductors and the effect of aging and solvent vapor annealing on the film structure. Through extensive X-ray structural investigations of spin coated films, we find a SIP with a significantly different structure to that found in single crystals of the same material forms; the SIP has a herringbone motif while single crystals display layered $\pi-\pi$ stacking. Over time, the structure of the film is found to slowly convert to the single crystal structure. Solvent vapor annealing initiates the same structural evolution process but at a greatly increased rate, and near complete conversion can be achieved in a short period of time. As properties such as charge transport capability are determined by the molecular structure, this work highlights the importance of understanding and controlling the structure of organic semiconductor films and presents a simple method to control the film structure by solvent vapor annealing.

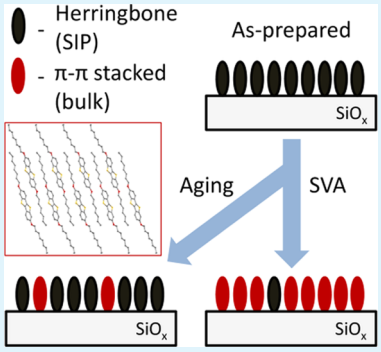

KEYWORDS: *organic electronics, X-ray diffraction, substrate-induced phase, polymorphism, organic thin films*

INTRODUCTION

In the field of organic electronics, the dependence of charge-transport capabilities on molecular structure is well-established and consideration of the semiconductor molecular structure is a key aspect in the optimal design of organic field-effect transistors (OFETs).[1−4] As the majority of charge transport occurs within the first few molecular layers, knowledge and control of the molecular structure at the substrate−film interface is therefore of great importance when considering materials for OFETs.[5] It has been demonstrated that the structure close to the substrate is not always the same as that of the bulk and so-called thin film, surface-mediated, or substrate-induced phases (SIPs) may form.[6,7] These polymorphic phases, which are typically not found as single-crystal structures, were first observed in films of the prototypical organic semiconductor pentacene,[8−13] and have since been found in other systems.[14−20] In films of pentacene, the SIP is found to be less energetically favorable than the bulk phase in isolation, but is stabilized close to the substrate because of improved compatibility of the structure with the flat surface of the substrate, such that in the presence of the substrate it is the most stable form.[21,22] The structural difference between the SIPs and bulk phases of π-conjugated molecules is most often related to a small change in the tilt angle between the approximately upright-standing molecules and the substrate, resulting in more favorable molecule−substrate interactions and a decrease in the out-of-plane lattice spacing such that the two phases are similar but distinct from one another.[13,23,24] Moreover, SIPs are found to be present only up to a certain film thickness, after which the bulk form grows on top so that two phases coexist within a thick film.[15,23−25] It is therefore clear that the structure of the SIP may influence charge mobility and potential device performance when present due to its proximity to the substrate.

For solution-processed OFETs, other considerations are the various secondary effects (e.g., rapid solvent evaporation,

Received: October 31, 2014
Accepted: January 8, 2015
Published: January 8, 2015

DOI: 10.1021/am5075908
ACS Appl. Mater. Interfaces 2015, 7, 1868−1873

dewetting, etc.) which occur during coating and impact on the long-range molecular order.[26,27] This has led to the routine treatment of films postcoating, with a view to improving molecular ordering; thermal annealing, and more recently solvent vapor annealing (SVA),[28] are two examples of processes which may be utilized. The sometimes high temperatures required for thermal annealing can limit the choice of substrate and the choice of semiconducting material because of melting or thermal decomposition; this makes SVA an attractive proposition, as it is less harsh on the sensitive systems used in organic electronics. Furthermore, it has been demonstrated that use of a SVA processing step can lead to improved device performance when compared with using thermal annealing alone.[29] When applied to pentacene films displaying a SIP, thermal annealing or SVA initiates a conversion to the bulk form.[7,30,31] This shows further potential for annealing to not only increase long-range order but also to lead to a reorganization of molecules and potentially alter film properties significantly.

In this work, we investigate the possible presence of a SIP in films of a symmetrically alkylated [1]benzothieno[3,2-*b*]-benzothiophene (BTBT) derivative and the effect of time and SVA on the stability or evolution of the crystalline structure and morphology. Alkylated BTBT derivatives have shown great potential for use in air-stable, high performance, solution-processable OFETs.[32−38] Charge transport mobilities of up to 3.5 $cm^2 V^{-1} s^{-1}$ have been recorded for polycrystalline films of dioctyl-BTBT (C_8−BTBT-C_8),[34] with even higher values recorded for single crystals.[35,39] Modification of the alkyl chain length of symmetrically substituted BTBT cores does not alter the arrangement of these BTBT cores; symmetrically dialkylated derivatives are isostructural with a herringbone (HB) packing motif and no SIPs are currently known for this class of molecule.[33] The subject of this study, dioctyloxy-BTBT (C_8O-BTBT-OC_8) (Figure 1), has an oxygen atom added between the BTBT core and the alkyl chains to encourage a different packing motif;[40] we will investigate whether this structural change leads to the presence of a SIP, using a variety of techniques to determine the solid-state arrangement of molecules in spin-coated films.

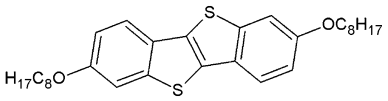

Figure 1. Molecular structure of C_8O-BTBT-OC_8.

EXPERIMENTAL SECTION

Synthesis of C_8O-BTBT-OC_8 is detailed in the Supporting Information.

Crystal Structure. Single crystals of C_8O-BTBT-OC_8 were grown by slow evaporation of unsaturated HPLC grade hexane solutions. X-ray diffraction data for crystals of the compound were collected at 123 K with graphite monochromated Mo Kα radiation (λ = 0.71073 Å) using an Oxford Diffraction Xcalibur E instrument. All non-hydrogen atoms were refined anisotropically. Hydrogen atoms were included in calculated positions utilizing riding modes. The structure was refined to convergence using all unique reflections and against F^2 with the SHELXL-97 program.[41] $C_{30}H_{40}O_2S_2$, M_r = 496.74, triclinic, space group $P\bar{1}$, a = 5.5225(4), b = 8.0712(4), c = 31.0578(15) Å, α = 94.482(4), β = 92.994(5), γ = 105.696(5)°, V = 1324.76(13) $Å^3$, Z = 2, μ = 0.226 mm^{-1}; $2\theta_{max}$ = 54.0°, 10939 reflections, 5633 unique, R_{int} = 0.0474; final refinement to convergence on F^2 gave R = 0.0537 (F, 4012 obs. data only) and R_w = 0.1040 (F^2, all data), GOF = 1.054. Detailed crystallographic data with refinement parameters are listed in complete crystallographic information files (CIF).

Polarized Optical Microscopy. Films were studied with a Nikon Eclipse E200 microscope equipped with a Nikon DS-Fi1 digital camera. Images were treated using the NIS-Elements software package (version 3.0).

Atomic Force Microscopy (AFM). Measurements were performed using a Nanosurf Easyscan 2 instrument in noncontact mode. A TAP 190 cantilever (Budgetsensors) with a nominal resonance frequency of 190 kHz was used. Data analysis and visualization were performed using the Gwyddion software package.[42]

Thin Film Preparation. Samples were prepared on silicon wafers (SIEGET WAFER Gmbh) with a 150 nm thick thermally grown oxide layer (SiO_x). Substrates were cleaned in an ultrasonic bath in acetone for 15 min and then isopropanol for a further 15 min, before drying with CO_2 gas. Films were prepared by spin-coating from chloroform solutions (150 μL, 10.8 mg mL^{-1}) at a rotation speed of 2500 rpm for 45s. Solutions were filtered through a 0.2 μL PTFE syringe filter immediately before film deposition. Films were solvent vapor annealed by placing the spin-coated film in a sealed glass beaker with chloroform solvent (50 mL) for 6 days.

X-ray Measurements. Specular X-ray diffraction (sXRD) measurements were performed on a PANalytical EMPYREAN reflectometer setup equipped with a copper sealed tube, a 1/32° primary slit, 10 mm beam mask and a multilayer mirror (λ = 1.54 Å) on the primary side. A receiving slit of 0.1 mm and a 3D PANalytical PIXcel detector were used on the secondary side. Grazing incidence X-ray diffraction (GIXD) measurements were performed at the BM25b beamline[43] at the ESRF (Grenoble, France) using X-rays with a wavelength of 0.9998 Å and an incident angle of α_i = 0.13°, just below the critical angle of the substrate. The sample was placed in a beryllium chamber[44] and data were collected under an N_2 gas flow. Diffracted intensities were measured using a 2D CCD area detector (Photonic Science Ltd.). Data were converted to reciprocal space maps using the in-house-developed software package PyGID, which was also used for peak indexation.[45] Additional GIXD measurements were conducted at BESSY II (Berlin, Germany) at the KMC-2 beamline using X-rays with a wavelength of 1.00 Å and a 2D cross-wire detector (BRUKER).[46] An incident angle of α_i = 0.13° was chosen to enhance the scattered intensities.To minimize the beam damage of the samples, we directly applied a constant flow of argon on the samples. The reciprocal space maps were calculated with the *xrayutilities* library for Python.[47]

RESULTS AND DISCUSSION

The single-crystal structure of C_8O-BTBT-OC_8 is shown in Figure 2 and the unit-cell parameters are displayed in Table 1. The structure is found to be layered, with slipped π−π stacking of the molecular cores and an interdigitation of molecules, in contrast to the HB motif displayed by other dialkylated BTBT derivatives (the unit-cell parameters of C_8-BTBT-C_8 are listed in Table 1).[33] This interdigitated structure could intuitively lead to an incompatibility with a flat surface so that, as in the case of pentacene, a different structure may form in the presence of a surface because of this incompatibility.[13,23,24]

C_8O-BTBT-OC_8 films were spin-coated from chloroform solution onto precleaned silicon wafers with a 150 nm layer of thermally grown oxide. AFM measurements (Figure 3a) and optical microscopy (see the Supporting Information) show that the as-prepared polycrystalline films are very rough with many individual crystallites visible; AFM measurements show a film thickness of approximately 65 nm with an average roughness of 18 nm. This thickness suggests the film is approximately 22 molecular layers thick, if molecules are standing upright with the long molecular axis perpendicular to the substrate (molecular length of 33.88 Å), as is commonly the case for films of rodlike conjugated molecules.[48]

DOI: 10.1021/am5075908
ACS Appl. Mater. Interfaces 2015, 7, 1868−1873

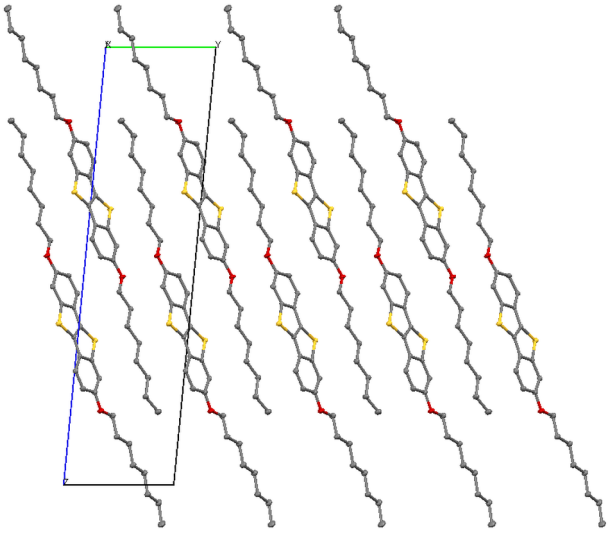

Figure 2. Single-crystal structure of C_8O-BTBT-OC_8 showing the unit cell and interdigitation of molecules. Hydrogen atoms have been removed for clarity.

Specular X-ray diffraction (sXRD) measurements, which measure only the lattice spacing perpendicular to the plane of the substrate, show several diffraction peaks (Figure 3c). The 001 reflection is observed at q_z = 0.20 Å^{-1}, along with higher order reflections, giving an out-of-plane lattice spacing of 30.85 Å. This is comparable to the 31.06 Å of the 001 of the bulk single-crystal structure but distinct; the *d*-spacing of 30.85 Å is close to the molecular length (33.88 Å) suggesting upright-standing molecules are present. This is very similar to other examples of SIPs such as pentacene, where only small changes in the out-of-plane lattice spacings occur even though a new molecular arrangement exists.[49]

Grazing incidence X-ray diffraction (GIXD) measurements were carried out to investigate the in-plane structure, i.e., the periodic packing within a sheet of C_8O-BTBT-OC_8, and the results show that the structure is in fact very different to that of the bulk. Films were first measured at the ESRF in Grenoble, France, and the same samples were then measured again 6 months later at BESSY II in Berlin, Germany. Peaks are observed along rods at q_{xy} = 1.34, 1.64, and 1.95 Å^{-1} at various q_z; none of these peaks should be present from the bulk structure and no other peaks are observed, showing a SIP has formed (Figure 4, left). The broadness of the peaks suggests that the crystalline domains are small. Using the unit cell of the known C_8–BTBT-C_8 structure (Table 1) as a starting point,[33] all diffraction peaks can be indexed by a slight adjustment of all unit cell parameters of this known structure; a monoclinic unit cell with two molecules in the asymmetric unit is able to explain the experimental GIXD pattern (Figure 4 and Table 1). The similarity of this unit cell to those of other dialkylated BTBT derivatives suggests that the SIP of C_8O-BTBT-OC_8 has molecules in a HB packing formation, in contrast to the layered, slipped π–π stacked structure observed in the bulk. Close packing is accepted to be the main driver in crystal structure formation and, therefore, the fact that the SIP is found to be less dense than the bulk structure (Table 1) may suggest that the SIP is a metastable form induced by the substrate.[50] It has not been possible to determine the exact HB angle or angle of tilt from the from these X-ray measurements, however, the strength of 020 reflection suggests that the BTBT cores (as the most electron dense fragments) are aligned approximately parallel to the *a*-axis in the 020 plane and that the difference between the out-of-plane lattice spacing and the molecular length likely arises from the alkyl chains bending away from the BTBT cores toward the substrate as opposed to a tilting of the core itself.

The measurements conducted 6 months later show a similar diffraction pattern, however, now with the addition of new peaks (Figure 4, middle). The SIP is still the dominant phase, while new peaks are visible at q_{xy} = 0.82, 1.16, and 1.66 Å^{-1} at various q_z. These new peaks can be assigned to the bulk structure and show an evolution from a metastable SIP toward the bulk has occurred over time. It is unclear if over a longer period of time the complete structure would convert to the bulk (including at the interface with the dielectric); even a slight conversion between forms could have a significant impact on the electronic properties and further underlines the importance of identifying and understanding SIPs.

With the presence of the SIP established, the effect of SVA on the film morphology and structure was investigated. Films were solvent annealed for 6 days using chloroform vapor. Long annealing times were chosen to ensure that samples had fully undergone any changes arising from the SVA process. AFM (Figure 3b) and optical microscopy (see the Supporting Information) measurements show significant changes to the film morphology. Larger domains of a regular shape are now present with a lower surface coverage and exposed (molecule free) substrate. sXRD measurements (Figure 3c) show only a small change in the out-of-plane structure (lattice spacing of 31.10 Å), whereas sharper diffraction peaks and the regular shape of domains indicate improved film crystallinity.

GIXD measurements after SVA reveal a large number of new peaks. Many of these peaks are affected by splitting, making interpretation of the data more difficult. Despite this difficulty, it is clear that the bulk structure dominates and peaks at 0.82, 1.18, 1.58, and 1.66 Å^{-1} in q_{xy} can be indexed with the bulk unit cell (Table 1 and Figure 4, right). This shows that the SVA process has induced a conversion from the SIP to the bulk phase, effectively the same process which occurs due to aging but at a significantly increased rate. The conversion may, however, not be complete and peaks at 1.62 Å^{-1} in q_{xy} could correspond to the bulk or the SIP. There are also peaks present at 1.20 and 1.54 Å^{-1} in q_{xy} that cannot be indexed using the two, now known, structures of C_8O-BTBT-OC_8. These peaks

Table 1. Unit-Cell Parameters of the Different Crystal Phases of C_8O-BTBT-OC_8 and the Related C_8-BTBT-C_8

sample	*a* (Å)	*b* (Å)	*c* (Å)	*α* (deg)	*β* (deg)	*γ* (deg)	*ρ* (g cm^{-3})
C_8O-BTBT-OC_8 Single X-tal[a]	5.5225(4)	8.0712(4)	31.058(2)	94.482(4)	92.994(5)	105.696(5)	1.245
C_8O-BTBT-OC_8 Bulk SVA[b]	5.56	8.27	30.89	96.50	93.00	107.80	1.233
C_8O-BTBT-OC_8 SIP	6.02	7.75	31.08	90	97.00	90	1.146
C_8–BTBT-C_8[33]	5.927(7)	7.88(1)	29.18(4)	90	92.443(4)	90	1.133

[a]Single-crystal data collected at 123 K. [b]Film measured at room temperature.

DOI: 10.1021/am5075908
ACS Appl. Mater. Interfaces 2015, 7, 1868–1873

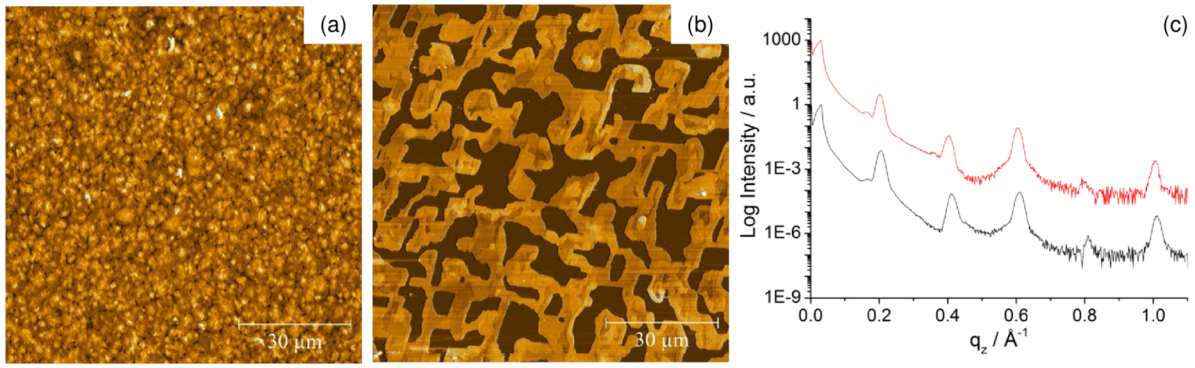

Figure 3. AFM images of (a) as-prepared and (b) solvent-annealed films and (c) sXRD patterns of the same as-prepared (black) and solvent annealed (red) films.

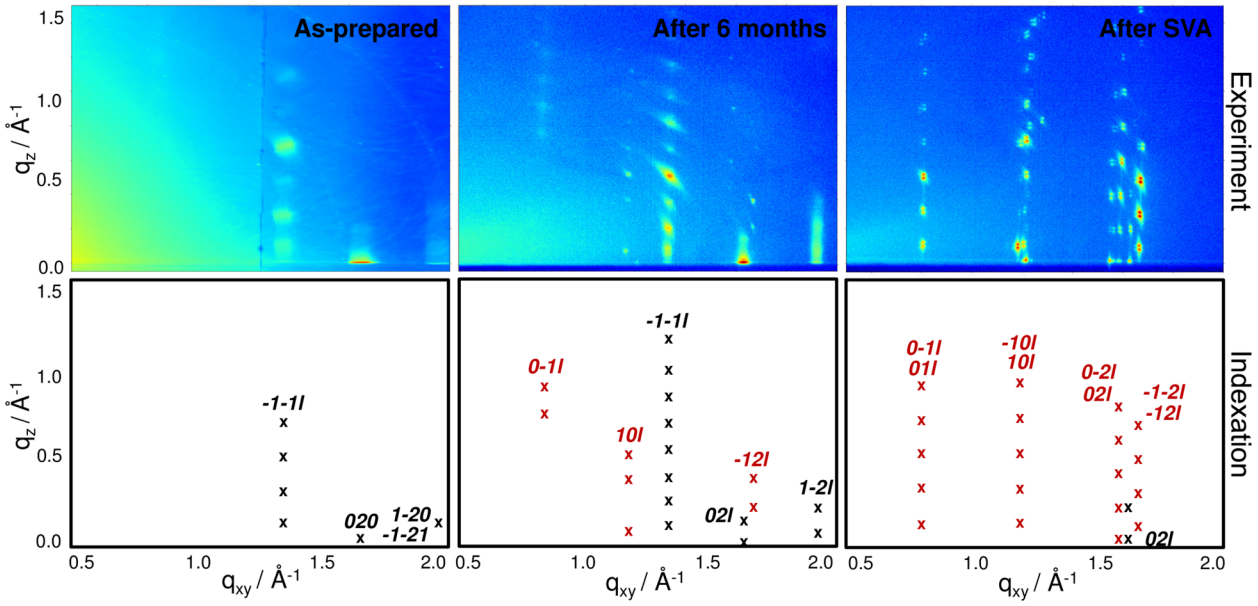

Figure 4. Experimental GIXD patterns of C_8O-BTBT-OC_8 films (above) and the corresponding peak indexation (below). Black crosses show peaks belonging to the SIP, whereas red crosses belong to the bulk phase.

could arise from a third, unknown, polymorphic phase or they could be the result of a supercell of either the SIP or the bulk phase, as a doubling of the in-plane lattice parameters of either phase can then account for these peaks and was also observed for a similar system previously.[15]

Films were also prepared from *o*-xylene solutions using the same preparation parameters (solution concentration, spin-coating speed, etc.). Optical microscopy, AFM, sXRD, and GIXD data are presented in the Supporting Information. The films display the same behavior as those described above, with a SIP transforming into the bulk by long time aging and more rapidly by SVA. This shows that, in the case of C_8O-BTBT-OC_8 on silica, the choice of solvent during preparation does not have an effect on the crystal structure of resultant films, and an SIP still forms regardless.

CONCLUSIONS

In conclusion, we have presented a detailed structural investigation of spin-coated films of C_8O-BTBT-OC_8 on a solid silica surface. A SIP with a HB packing motif is formed, in contrast to the slipped $\pi-\pi$ stacking of the bulk, and the same structure persists regardless of the solvent used during sample preparation. Over 6 months, the SIP structure slowly evolves toward that of the bulk. Using SVA, the rate of conversion to the bulk can be greatly increased and gives almost complete conversion within a few days, providing a simple method to switch from the SIP to the bulk polymorph. Furthermore, this is the first example of a SIP that has a completely different packing arrangement from that of the bulk and is not only related to a change in the molecular tilt of the core typically responsible for the charge transport. This work emphasizes the importance of SIPs when dealing with organic electronics and shows the potential for SVA to be used for polymorph selection.

ASSOCIATED CONTENT

Supporting Information

Synthesis of C_8O-BTBT-OC_8. Crystallographic information file for C_8O-BTBT-OC_8. Optical microscopy data of films produced from chloroform solution. Optical microscopy, AFM, sXRD, and GIXD data of films produced from *o*-xylene solutions. This material is available free of charge via the Internet at http://pubs.acs.org.

DOI: 10.1021/am5075908
ACS Appl. Mater. Interfaces 2015, 7, 1868−1873

AUTHOR INFORMATION

Corresponding Author

*E-mail: andrew.jones@tugraz.at.

Notes

The authors declare no competing financial interest.

ACKNOWLEDGMENTS

The authors acknowledge financial support from the ARC program of the Communauté Française de Belgique (Grant 20061) and from the Walloon Region (WCS project 1117306). Y.H.G. benefits from a mandate of Francqui Research Professor.

REFERENCES

(1) Dinelli, F.; Murgia, M.; Levy, P.; Cavallini, M.; Biscarini, F.; de Leeuw, D. M. Spatially Correlated Charge Transport in Organic Thin Film Transistors. *Phys. Rev. Lett.* **2004**, *92*, 116802.

(2) Coropceanu, V.; Cornil, J.; da Silva Filho, D. A.; Olivier, Y.; Silbey, R.; Brédas, J.-L. Charge Transport in Organic Semiconductors. *Chem. Rev.* **2007**, *107*, 926−952.

(3) Mas-Torrent, M.; Rovira, C. Role of Molecular Order and Solid-State Structure in Organic Field-Effect Transistors. *Chem. Rev.* **2011**, *111*, 4833−4856.

(4) Schweicher, G.; Olivier, Y.; Lemaur, V.; Geerts, Y. H. What Currently Limits Charge Carrier Mobility in Crystals of Molecular Semiconductors? *Isr. J. Chem.* **2014**, *54*, 595−620.

(5) Wang, C.; Dong, H.; Hu, W.; Liu, Y.; Zhu, D. Semiconducting π-Conjugated Systems in Field-Effect Transistors: A Material Odyssey of Organic Electronics. *Chem. Rev.* **2012**, *112*, 2208−2267.

(6) Bouchoms, I. P. M.; Schoonveld, W. A.; Vrijmoeth, J.; Klapwijk, T. M. Morphology Identification of the Thin Film Phases of Vacuum Evaporated Pentacene on SiO_2 Substrates. *Synth. Met.* **1999**, *104*, 175−178.

(7) Mattheus, C. C.; Dros, A. B.; Baas, J.; Oostergetel, G. T.; Meetsma, A.; de Boer, J. L.; Palstra, T. T. M. Identification of Polymorphs of Pentacene. *Synth. Met.* **2003**, *138*, 475−481.

(8) Fritz, S. E.; Martin, S. M.; Frisbie, C. D.; Ward, M. D.; Toney, M. F. Structural Characterization of a Pentacene Monolayer on an Amorphous SiO_2 Substrate with Grazing Incidence X-ray Diffraction. *J. Am. Chem. Soc.* **2004**, *126*, 4084−4085.

(9) Nabok, D.; Puschnig, P.; Ambrosch-Draxl, C.; Werzer, O.; Resel, R.; Smilgies, D.-M. Crystal and Electronic Structures of Pentacene Thin Films from Grazing-Incidence X-Ray Diffraction and First-Principles Calculations. *Phys. Rev. B* **2007**, *76*, 235322.

(10) Yoshida, H.; Inaba, K.; Sato, N. X-Ray Diffraction Reciprocal Space Mapping Study of the Thin Film Phase of Pentacene. *Appl. Phys. Lett.* **2007**, *90*, 181930.

(11) Schiefer, S.; Huth, M.; Dobrinevski, A.; Nickel, B. Determination of the Crystal Structure of Substrate-Induced Pentacene Polymorphs in Fiber Structured Thin Films. *J. Am. Chem. Soc.* **2007**, *129*, 10316−10317.

(12) Yoshida, H.; Sato, N. Crystallographic and Electronic Structures of Three Different Polymorphs of Pentacene. *Phys. Rev. B* **2008**, *77*, 235205.

(13) Mannsfeld, S. C. B.; Virkar, A.; Reese, C.; Toney, M. F.; Bao, Z. Precise Structure of Pentacene Monolayers on Amorphous Silicon Oxide and Relation to Charge Transport. *Adv. Mater.* **2009**, *21*, 2294−2298.

(14) Wedl, B.; Resel, R.; Leising, G.; Kunert, B.; Salzmann, I.; Oehzelt, M.; Koch, N.; Vollmer, A.; Duhm, S.; Werzer, O.; Gbabode, G.; Sferrazza, M.; Geerts, Y. Crystallisation Kinetics in Thin Films of Dihexyl-Terthiophene: The Appearance of Polymorphic Phases. *RSC Adv.* **2012**, *2*, 4404−4414.

(15) Werzer, O.; Boucher, N.; de Silva, J. P.; Gbabode, G.; Geerts, Y. H.; Konovalov, O.; Moser, A.; Novak, J.; Resel, R.; Sferrazza, M. Interface Induced Crystal Structures of Dioctyl-Terthiophene Thin Films. *Langmuir* **2012**, *28*, 8530−8536.

(16) Giri, G.; Verploegen, E.; Mannsfeld, S. C. B.; Atahan-Evrenk, S.; Kim, D. H.; Lee, S. Y.; Becerril, H. A.; Aspuru-Guzik, A.; Toney, M. F.; Bao, Z. Tuning Charge Transport in Solution-Sheared Organic Semiconductors Using Lattice Strain. *Nature* **2011**, *480*, 504−508.

(17) Salzmann, I.; Nabok, D.; Oehzelt, M.; Duhm, S.; Moser, A.; Heimel, G.; Puschnig, P.; Ambrosch-Draxl, C.; Rabe, J. P.; Koch, N. Structure Solution of the 6,13-Pentacenequinone Surface-Induced Polymorph by Combining X-Ray Diffraction Reciprocal-Space Mapping and Theoretical Structure Modeling. *Cryst. Growth Des.* **2011**, *11*, 600−606.

(18) Gbabode, G.; Dumont, N.; Quist, F.; Schweicher, G.; Moser, A.; Viville, P.; Lazzaroni, R.; Geerts, Y. H. Substrate-Induced Crystal Plastic Phase of a Discotic Liquid Crystal. *Adv. Mater.* **2012**, *24*, 658−662.

(19) Lercher, C.; Resel, R.; Balandier, J.-Y.; Niebel, C.; Geerts, Y. H.; Sferrazza, M.; Gbabode, G. Effects of Temperature on the Polymorphism of α,ω-Dioctylterthiophene in Thin Films. *J. Cryst. Growth* **2014**, *386*, 128−134.

(20) Chattopadhyay, B.; Ruzié, C.; Resel, R.; Henri Geerts, Y. Substrate-Induced Phases: Transition from a Liquid-Crystalline to a Plastic Crystalline Phase via Nucleation Initiated by the Substrate. *Liq. Cryst.* **2014**, *41*, 302−309.

(21) Della Valle, R. G.; Venuti, E.; Brillante, A.; Girlando, A. Molecular Dynamics Simulations for a Pentacene Monolayer on Amorphous Silica. *ChemPhysChem* **2009**, *10*, 1783−1788.

(22) Yoneya, M.; Kawasaki, M.; Ando, M. Molecular Dynamics Simulations of Pentacene Thin Films: The Effect of Surface on Polymorph Selection. *J. Mater. Chem.* **2010**, *20*, 10397−10402.

(23) Drummy, L. F.; Martin, D. C. Thickness-Driven Orthorhombic to Triclinic Phase Transformation in Pentacene Thin Films. *Adv. Mater.* **2005**, *17*, 903−907.

(24) Cheng, H.-L.; Mai, Y.-S.; Chou, W.-Y.; Chang, L.-R.; Liang, X.-W. Thickness-Dependent Structural Evolutions and Growth Models in Relation to Carrier Transport Properties in Polycrystalline Pentacene Thin Films. *Adv. Funct. Mater.* **2007**, *17*, 3639−3649.

(25) Knipp, D.; Street, R. A.; Völkel, A.; Ho, J. Pentacene Thin Film Transistors on Inorganic Dielectrics: Morphology, Structural Properties, and Electronic Transport. *J. Appl. Phys.* **2003**, *93*, 347−355.

(26) Dickey, K. C.; Anthony, J. E.; Loo, Y.-L. Improving Organic Thin-Film Transistor Performance through Solvent-Vapor Annealing of Solution-Processable Triethylsilylethynyl Anthradithiophene. *Adv. Mater.* **2006**, *18*, 1721−1726.

(27) Palermo, V.; Samorì, P. Molecular Self-Assembly across Multiple Length Scales. *Angew. Chem., Int. Ed.* **2007**, *46*, 4428−4432.

(28) Luca, G. D.; Treossi, E.; Liscio, A.; Mativetsky, J. M.; Scolaro, L. M.; Palermo, V.; Samorì, P. Solvent Vapour Annealing of Organic Thin Films: Controlling the Self-Assembly of Functional Systems across Multiple Length Scales. *J. Mater. Chem.* **2010**, *20*, 2493−2498.

(29) Zhao, Y.; Xie, Z.; Qu, Y.; Geng, Y.; Wang, L. Solvent-Vapor Treatment Induced Performance Enhancement of poly(3-Hexylthiophene):methanofullerene Bulk-Heterojunction Photovoltaic Cells. *Appl. Phys. Lett.* **2007**, *90*, 043504.

(30) Amassian, A.; Pozdin, V. A.; Li, R.; Smilgies, D.-M.; Malliaras, G. G. Solvent Vapor Annealing of an Insoluble Molecular Semiconductor. *J. Mater. Chem.* **2010**, *20*, 2623−2629.

(31) Moser, A.; Novák, J.; Flesch, H.-G.; Djuric, T.; Werzer, O.; Haase, A.; Resel, R. Temperature Stability of the Pentacene Thin-Film Phase. *Appl. Phys. Lett.* **2011**, *99*, 221911.

(32) Ebata, H.; Izawa, T.; Miyazaki, E.; Takimiya, K.; Ikeda, M.; Kuwabara, H.; Yui, T. Highly Soluble [1]Benzothieno[3,2-B]-benzothiophene (BTBT) Derivatives for High-Performance, Solution-Processed Organic Field-Effect Transistors. *J. Am. Chem. Soc.* **2007**, *129*, 15732−15733.

(33) Izawa, T.; Miyazaki, E.; Takimiya, K. Molecular Ordering of High-Performance Soluble Molecular Semiconductors and Re-Evaluation of Their Field-Effect Transistor Characteristics. *Adv. Mater.* **2008**, *20*, 3388−3392.

(34) Liu, C.; Minari, T.; Lu, X.; Kumatani, A.; Takimiya, K.; Tsukagoshi, K. Solution-Processable Organic Single Crystals with

DOI: 10.1021/am5075908
ACS Appl. Mater. Interfaces 2015, 7, 1868−1873

Bandlike Transport in Field-Effect Transistors. *Adv. Mater.* **2011**, *23*, 523−526.
(35) Minemawari, H.; Yamada, T.; Matsui, H.; Tsutsumi, J.; Haas, S.; Chiba, R.; Kumai, R.; Hasegawa, T. Inkjet Printing of Single-Crystal Films. *Nature* **2011**, *475*, 364−367.
(36) Amin, A. Y.; Reuter, K.; Meyer-Friedrichsen, T.; Halik, M. Interface Engineering in High-Performance Low-Voltage Organic Thin-Film Transistors Based on 2,7-Dialkyl-[1]benzothieno[3,2-b][1]benzothiophenes. *Langmuir* **2011**, *27*, 15340−15344.
(37) Amin, A. Y.; Khassanov, A.; Reuter, K.; Meyer-Friedrichsen, T.; Halik, M. Low-Voltage Organic Field Effect Transistors with a 2-Tridecyl[1]benzothieno[3,2-b][1]benzothiophene Semiconductor Layer. *J. Am. Chem. Soc.* **2012**, *134*, 16548−16550.
(38) Colella, S.; Ruzié, C.; Schweicher, G.; Arlin, J.-B.; Karpinska, J.; Geerts, Y.; Samorì, P. High Mobility in Solution-Processed 2,7-Dialkyl-[1]benzothieno[3,2-b][1]benzothiophene-Based Field-Effect Transistors Prepared with a Simplified Deposition Method. *ChemPlusChem.* **2014**, *79*, 371−374.
(39) Yuan, Y.; Giri, G.; Ayzner, A. L.; Zoombelt, A. P.; Mannsfeld, S. C. B.; Chen, J.; Nordlund, D.; Toney, M. F.; Huang, J.; Bao, Z. Ultra-High Mobility Transparent Organic Thin Film Transistors Grown by an off-Centre Spin-Coating Method. *Nat. Commun.* **2014**, *5*, 3005.
(40) Elemans, J. A. A. W.; Lei, S.; De Feyter, S. Molecular and Supramolecular Networks on Surfaces: From Two-Dimensional Crystal Engineering to Reactivity. *Angew. Chem., Int. Ed.* **2009**, *48*, 7298−7332.
(41) Sheldrick, G. M. A Short History of *SHELX*. *Acta Crystallogr., Sect. A* **2008**, *64*, 112−122.
(42) Nečas, D.; Klapetek, P. Gwyddion: An Open-Source Software for SPM Data Analysis. *Cent. Eur. J. Phys.* **2012**, *10*, 181−188.
(43) Rubio-Zuazo, J.; Ferrer, P.; López, A.; Gutiérrez-León, A.; da Silva, I.; Castro, G. R. The Multipurpose X-Ray Diffraction End-Station of the BM25B-SpLine Synchrotron Beamline at the ESRF. *Nucl. Instrum. Methods Phys. Res., Sect. A* **2013**, *716*, 23−28.
(44) Ferrer, P.; Rubio-Zuazo, J.; Heyman, C.; Esteban-Betegón, F.; Castro, G. R. Multi-Use High/low-Temperature and Pressure Compatible Portable Chamber for *in Situ* Grazing-Incidence X-Ray Scattering Studies. *J. Synchrotron Radiat.* **2013**, *20*, 474−481.
(45) Moser, A. Crystal Structure Solution Based on Grazing Incidence X-ray Diffraction: Software Development and Application to Organic Films. *Ph.D. Thesis*, Graz University of Technology, Graz, Austria, 2012.
(46) Erko, A.; Packe, I.; Hellwig, C.; Fieber-Erdmann, M.; Pawlizki, O.; Veldkamp, M.; Gudat, W. KMC-2: The New X-Ray Beamline at BESSY II. In *AIP Conference Proceedings*; AIP Publishing: Melville, NY, 2000; Vol. *521*, pp 415−418.
(47) Kriegner, D.; Wintersberger, E.; Stangl, J. *xrayutilities*: A Versatile Tool for Reciprocal Space Conversion of Scattering Data Recorded with Linear and Area Detectors. *J. Appl. Crystallogr.* **2013**, *46*, 1162−1170.
(48) Hlawacek, G.; Teichert, C. Nucleation and Growth of Thin Films of Rod-like Conjugated Molecules. *J. Phys.: Condens. Matter* **2013**, *25*, 143202.
(49) Werzer, O.; Stadlober, B.; Haase, A.; Oehzelt, M.; Resel, R. Full X-Ray Pattern Analysis of Vacuum Deposited Pentacene Thin Films. *Eur. Phys. J. B* **2008**, *66*, 455−459.
(50) Burger, A.; Ramberger, R. On the Polymorphism of Pharmaceuticals and Other Molecular Crystals. II. *Microchim. Acta* **1979**, *72*, 273−316.

DOI: 10.1021/am5075908
ACS Appl. Mater. Interfaces 2015, 7, 1868−1873